HHS Public Access

Author manuscript

Cancer Immunol Res. Author manuscript; available in PMC 2022 August 04.

Published in final edited form as:

Cancer Immunol Res. 2022 February ; 10(2): 245–258. doi:10.1158/2326-6066.CIR-21-0435.

C3aR Signaling Inhibits NK-cell Infiltration into the Tumor Microenvironment in Mouse Models

Saravanan Nandagopal[1], **Caiyun G. Li**[1], **Yu Xu**[2], **Quaovi H. Sodji**[1], **Edward E. Graves**[1], **Amato J. Giaccia**[1,3,*]

[1]Department of Radiation Oncology, Stanford University School of Medicine, Stanford, CA 94305, USA.

[2]Department of Bioengineering, Stanford, CA 94305, USA.

[3]MRC/CRUK Oxford Institute for Radiation Oncology and Gray Laboratory, University of Oxford, Old Road Campus Research Building, Roosevelt Drive, Oxford OX3 7DQ, UK.

Abstract

Many solid tumors have low levels of cytotoxic CD56^{dim} NK cells, suggesting that CD56^{dim} NK-cell exclusion from the tumor microenvironment (TME) contributes to the decreased response rate of immunotherapy. Complement component 3a (C3a) is known for its tumor-promoting and immunosuppressive roles in solid tumors. Previous reports have implicated the involvement of the C3a receptor (C3aR) in immune cell trafficking into the TME. C3aR is predominantly expressed on the surface of activated cytotoxic NK cells, but a specific role for C3aR in NK-cell biology has not been investigated. Because solid tumors generate elevated C3a and have decreased NK cell infiltration, we hypothesized that C3aR might play a role in cytotoxic NK-cell recruitment into the TME. Our results indicate that blocking C3aR signaling in NK cells increased NK-cell infiltration into the TME in mouse models and led to tumor regression. Because the critical lymphocyte trafficking integrin, LFA-1, orchestrates the migration of activated NK cells, we wanted to gain insight into the interaction between C3aR signaling and LFA-1. Our results demonstrated that direct interaction between C3aR and LFA-1, which led to a high affinity LFA-1 conformation, decreased NK-cell infiltration into the TME. We propose that approaches to enhance cytotoxic NK-cell infiltration into the TME, through either disrupting C3a and C3aR interaction or inhibiting the formation of high-affinity LFA-1, represents a new strategy to improve the efficiency of immunotherapy for cancer treatment.

*Corresponding author: giaccia@stanford.edu, amato.giaccia@oncology.ox.ac.uk.

Author contributions

S.N. conceived the hypothesis and project. S.N., E.G., and A.G. designed the project and experiments. S.N. performed the experiments, collected, and analyzed the results, interpreted data, and wrote the manuscript. C.G.L performed mouse immunoprecipitation. Y.X helped with animal experiments. Q.S helped with cytotoxic assays. E.G. and A.G. provided study funding, interpreted data, provided material support, and edited the manuscript.

The authors declare no conflict of interests.

Declaration of Interests

The authors declare no competing financial interests.

Keywords

NK cells; C3a; C3aR; Lymphocyte-function associated antigen 1 (LFA-1); Immunotherapy; Immune cell infiltration; CD11a; CD18

Introduction

Natural killer (NK) cells can mediate direct killing of transformed cells without prior antigenic exposure or priming (1). Efficient homing of NK cells into the tumor microenvironment (TME) is essential for effective tumor cell killing (2,3). NK-cell trafficking is controlled by various chemokines, complement fragments, and adhesion molecules (4–6). Therefore, impaired NK-cell trafficking would have a direct impact on an effective innate immune response against tumors (7).

Although the immune system is effective in limiting tumor cell growth and survival, tumor cells frequently develop immune evasion strategies that allow them to escape from immune-mediated killing, particularly from NK cells. Studies have shown that NK cell numbers are reduced in malignant tissues compared to non-malignant tissues, and that tumors with infiltrating NK cells correlate with a better prognosis (2,8,9). Analysis of the NK cells found in the TME of many solid tumors is dominated by non-cytotoxic, cytokine-producing $CD56^{bright}$ NK cells rather than cytotoxic $CD56^{dim}$ NK cells, providing an explanation for ineffective NK-cell control of tumor growth (9). Therefore, approaches to enhance cytotoxic NK-cell infiltration into the TME represents a reasonable strategy to control tumor growth and progression.

Tumor-derived C3a (complement component 3a) is implicated in the immunosuppression, growth, and inflammation of various tumor models (10). C3a plays a critical role in the recruitment of leukocytes into the TME (11). In contrast, the role of C3a on NK-cell infiltration into tumors and NK-cell anti-tumor activity has not been previously explored. Cytotoxic $CD56^{dim}$ NK cells show increased C3aR expression compared to cytokine-producing $CD56^{bright}$ NK cells (12). However, little is known mechanistically about how C3a and its receptor, C3aR, regulate cytotoxic NK-cell recruitment and activity in solid tumors.

C3aR is a G-protein coupled receptor (GPCR), and GPCR stimulation can induce activation of integrin molecules (13). Integrins play important roles in immune cell extravasation, infiltration, and homeostasis (14,15). For example, the conformational state of lymphocyte function-associated antigen-1 (LFA-1 or $\alpha_L\beta_2$; CD11a/CD18) regulates immune cell migration, extravasation, and activation (15–17). Earlier reports demonstrate an increased expression of LFA-1 in NK cells and decreased expression of other β_2 integrin receptors, such as CD11b/CD18 (CR3) and CD11c/CD18 (CR4)(18,19). Higher expression of LFA-1 is found in the cytotoxic $CD56^{dim}$ NK subset compared to $CD56^{bright}$ NK subset and T cells (20). The increased expression of LFA-1 is important because adhesion and migration of IL2-activated NK cells are modulated by LFA-1 (19,21,22). Interestingly, $CD56^{dim}$ NK cells also show increased expression of C3aR compared to $CD56^{bright}$ NK cells (12). The

interaction between C3aR and LFA-1 in regulating cytotoxic NK-cell infiltration into tumors has not been rigorously explored.

This study investigated the role of the C3aR on NK-cell infiltration into the TME. The interaction between C3aR and LFA-1 in modulating LFA-1 conformation and its contribution to tumor evasion from NK-cell immunosurveillance was also investigated in preclinical models. These studies provide evidence that inhibition of C3aR activation or disruption of LFA-1 conformational changes can lead to increased infiltration of NK cells and effective immunotherapy.

Materials and Methods

Details about the reagents used in this study can be found in the Supplementary Table.

Animals

All procedures involving animals and their care were approved by the Institutional Animal Care and Use Committee of Stanford University in accordance with institutional and NIH guidelines. 6–8-week-old female C57BL6, Balb/c, and C3aR-knockout (KO) mice were used in all experiments. C57BL6 (Strain code 027) and Balb/c (Starin code 028) mice were purchased from Charles River. C3aR KO animals were purchased from Jackson laboratory (stock no. 005712). Animals were housed for one week to acclimate prior to the commencement of experimental procedures. All animal experiments were performed according to institutional guidelines and approved animal protocol. Power calculation and experimental models from previous publications were used as reference to determine the sample size.

Human and mouse NK cell isolation

Blood samples from anonymous healthy donors were obtained from Stanford Blood center and used to isolare NK cells. Human total peripheral blood mononuclear cells (PBMCs) were collected by density-gradient centrifugation using Ficoll-Paque PLUS (Cat# 17–1440-02, GE Healthcare, Sweden). The manufacturer’s protocol was followed to separate NK cells from total PBMCs using the EasySep human NK Negative Selection Kit (Cat# 19055, StemCell Technologies, Vancouver, BC, Canada). Mouse NK cells were isolated from splenocytes using Ficoll-Paque premium (Cat# 17–5446-02, GE Healthcare, Sweden) and EasySep mouse NK Negative Selection Kit (Cat# 19755 and 19855, StemCell Technologies, Vancouver, BC, Canada). Purified NK cells were incubated in supplemented RPMI-1640 (Gibco, Cat# 3180089) supplemented with 10% fetal bovine serum (FBS; Omega Sci. Cat# FB-02), 1% penicillin/streptomycin (Gibco, 15140122) and L-Glutamine (Gibco, Cat# 25030081) and containing 1000 units/mL recombinant human (rh)IL2 (Cat# 200–02, PeproTech, USA) at 37 °C and 5% CO2 for four days before use.

Cell culture

Human cancer cell lines MDA-MB-231, MCF7, BT474, HCC1143, T47D, AU565, and HCT116 were obtained from ATCC and used within 1 year of purchase. Cells were cultured in supplemented DMEM (Gibco, Cat# 12800082) containing 10% FBS, 1% penicillin/

streptomycin, and L-Glutamine. Mouse cancer cell lines MC38, EO771 (courtesy of Peter MacCallum Cancer Institute and Olivia Newton-John Cancer Research Institute, Australia), CT26 (courtesy of Matt Bogyo, Stanford University), and JC (courtesy of Dr. Chris Contag, Michigan State University) were cultured in supplemented RPMI (10% FBS, 1% penicillin/streptomycin/L-glutamine). Cells were cultured at 37°C and 5% CO_2. Cell lines were authenticated (STR), and cultures were checked regularly to ensure no mycoplasma contamination (Lonza Cat# LT 07–318).

Transwell assays

50 μg fibronectin (Corning, Cat# 354008) from stock solution (1 mg/mL) was mixed with 950 μL migration medium (RPMI with 1% BSA (Sigma-Aldrich, Cat# A7030). 5 μM pore size, 6.5 mm diameter transwell inserts (Corning, Cat# 3421) were coated with 50 μL of fibronectin and incubated for one hour at room temperature. Excessive fibronectin was pipetted off carefully without damaging the inserts. Blocking was achieved with 50 μL of migration medium for 30 minutes incubation at room temperature. Excessive blocking solution was pipetted off carefully. 600 μL control migration medium or chemoattractant [MCP-1 or SDF (stromal-derived factor-1)] supplemented media or cancer cell-conditioned media (conditioned media were obtained from 90% confluency of corresponding cancer cell culture) was added to the bottom well. The coated inserts were placed carefully into the transwells, and isolated human or mouse NK cells in 100 μL of migration medium were placed in the top well. For control experiments, 5 nM human MCP-1, 100 ng/mL mouse SDF-1, and 2 μg/mL C3a were used. Cultures were incubated at 37°C and 5% CO_2 for two hours to allow for NK-cell migration. After incubation, inserts were removed carefully, and the bottom well content was suspended using micropipette for uniform distribution of migrated cells. Cells were counted using a hemocytometer, and the migrated cells were normalized to the input cell number and percentage of migration was calculated.

Mouse models

For C3aR inhibitor study, one million cells of the cancer cell line EO771 were injected orthotopically in the mammary fat pad of C57BL/6 or one million cells of the cancer cell line MC38 were injected subcutaneously into the flank of C57BL/6 mice. Animals were checked every 24 hours. Animal weight and tumor size were measured using weighing balance and caliper, respectively. Inhibitor treatment was started once tumors reached approximately 100 mm^3 in size. Randomization of animals was done to ensure approximately equal size of tumors in the different treatment groups. The working concentration of the C3aR-specific inhibitor SB-290157 (TOCRIS, Cat# 6860) was 10 mg/kg in 90% PBS, 5% DMSO, and 5% ethanol, which was prepared from a stock solution of 20 mg/mL in DMSO. When tumor volume reached 100 mm^3, SB-290157 was intraperitonially administered once every 12 hours as described previously (23). Control animals were treated with vehicle (90% PBS, 5% DMSO, and 5% ethanol). After five days of treatment, animals were sacrificed, and tumor tissues were collected and processed (described below) for analysis.

For the NK depletion study, the subcutaneous MC38 model was used. 150 μg anti-NK1.1 (BioXcell, Cat# BEOO36) or IgG control (BioXcell, Cat# BEOO85) was administered to

deplete NK cells two days prior to tumor cell inoculation, the day of tumor cell inoculation, and every fourth day after tumor inoculation. SB-290157 was administered as described above to the IgG control and NK1.1-depleted groups once the tumors reached 100 mm^3. We also used 30 μL rabbit polyclonal anti-asialo-GM1(FUJIFILM Wako Pure Chemicals Corporations Cat# 986–10001) to deplete NK cells in C3aR-KO mice. Anti-asialo-GM1 or saline was injected intraperitoneally one day prior to, and on the day of, tumor cell inoculation as well as every fifth day after tumor inoculation.

To test a syngeneic model in BALB/c mice, CT26 cells (10^6 in 50 μL of PBS) were injected subcutaneously into the flanks of BALB/c wild-type or C3aR-KO animals. JC cells (10^6 in 50 μL of PBS) were administered orthotopically into to the mammary fat pad of BALB/c wild-type or C3aR-KO mice.

In vivo inhibition of LFA-1 was performed through intraperitoneal administration of 30 μL of BIRT377 (TOCRIS, Cat# 4776) dissolved in DMSO on alternate days beginning once the tumors reached a volume of 100 mm^3. Control mice were administered an equal volume of vehicle (DMSO). After four doses (post tumor injection days: 12, 14, 16, and 18), animals were sacrificed, and tumor tissues were collected and processed as described below for further analysis.

Tumor tissue processing

Tumor samples were collected in 5 mL of ice-cold serum free RPMI. Samples were chopped using a razor blade and collected in 50 mL conical tubes, and the solution volume was adjusted to 5 mL with ice cold RPMI. 20μL of liberase (Cat# 5401020001, Sigma-Aldrich) and 20μL of DNase (Cat# D4527–10KU, Sigma-Aldrich)(20 μL for every 5 mL sample) were added to each sample and kept in a shaker for 40 minutes (225 rpm at 37ºC). The enzymatic reaction was terminated after 40 minutes by adding 10 mL of ice cold RPMI supplemented with 10% FBS. Dissociated tissue samples were mashed through 40 μm sterile nylon strainer (Cat# 431750, Corning USA) using a 5 mL syringe. The collected cells were centrifuged with excess RPMI medium at 1500 rpm for 10 minutes. The cell pellets were then processed for flow cytometry analysis.

Flow cytometry

Freshly isolated or IL2-activated human or mouse NK cells, or extracted cells obtained from tumor tissues, were washed twice with FACS buffer [PBS supplemented with 1 % BSA (Sigma-Aldrich, Cat# A7030)]. Fc blocking was done for 10 minutes at 4°C. Antibodies or isotype controls were added, and the samples were kept at 4°C in the dark for 45 minutes. The samples were washed with FACS buffer at 1500 rpm for 5 minutes, and the supernatant was discarded. The final volume was adjusted to 150 μL with FACS buffer before analysis. To identify the high-affinity status of LFA-1, an untagged primary antibody specific to epitope 24 (mAB24; Cat# 13219, abcam) and secondary antibody to mAB24 were used. Flow cytometry study was blinded during acquisition and analysis. Information about Fc blocking and primary/secondary antibodies are available in the Supplementary Table.

ELISAs

MDA MB-231, MCF7, BT474, HCC1143, T47D, AU565, and HCT116 were grown in phenol red-free DMEM (Gibco, Cat# 31053028) medium supplemented with 10% FBS and 1% antibiotic solution in T75 flasks. The supernatants were collected when the confluency reached 90%. The human C3a ELISA kit from Hycultbiotech (Cat# HK354–01) was used for C3a quantification according to the manufacturer's protocol.

NK-cell migration using a microfluidic platform and data analysis

"μ-slide chemotaxis" microfluidic devices (ibidi, Cat# 80326) were coated with fibronectin (50 μg/50 μL mixed with 950 μL of migration medium) and incubated at room temperature for one hour. The excessive fibronectin was removed, and the device was filled with 0.4% BSA in RPMI for blocking. The BSA-blocked device was kept at room temperature for 1 hour for further use. Meanwhile, microscopic stage (DMi8, Leica) temperature was maintained at 37˚C using Okolab microscope incubator for live cell imaging. NK cells (0.4 million cells for each experiment) were loaded into the middle inlet. Recombinant human (rh) C3a (R & D, Cat# 3677-C3–025) (2 μg/mL mixed with migration medium, 0.4% BSA in RPMI), conditioned medium from MDA MB-231, HCT116, and T47D, C3a-neutralized conditioned medium from MDA MB-231 and HCT116 (supernatant collected when the confluency is about 90%), or migration medium alone was infused into the device through 2 side inlets using 200 μL pipette. NK-cell migration was recorded by time-lapse microscopy at three frames/minute for 20 minutes under a Leica DMi8 using 10X object. The acquired images were analyzed using imageJ's (NIH open source) "analyze plugin-manual tracker" to obtain position of migration. The Chemotaxis and Migration tool was used to calculate the average velocity and cell tracks.

Immunofluorescence

IL2-activated human NK cells were attached in the microfluidic channel as described above and exposed to C3a-containing medium (2 μg/mL mixed with migration medium, 0.4% BSA in RPMI) or IgG control for 20 minutes. The cells were fixed [PFA 4% in PBS (Santa Cruz Biotechnology, Cat# 30525–89-4)], washed, and blocked with 10% goat serum (Thermofisher Scientific, Cat# 31872) for 45 minutes at room temperature. Primary rabbit anti-human CD11a (Cat#ab52895, Abcam, USA), primary rabbit anti-human CD18 (phospo-T758; Cat#ab63388, Abcam, USA), primary mouse anti-human CD11a+CD18 antibody [24] (Cat# ab13219, Abcam, USA), or respective control antibody (Rabbit IgG and Mouse IgG1) was diluted as suggested by the provider, infused into the microfluidic devices, and incubated for overnight at 4^{o}C. Samples were then washed three times and incubated with diluted secondary antibody (1:200 dilution; anti-mouse goat IgG, Cat# A32723 or anti-rabbit goat IgG, Cat# A32721, Thermofisher Scientific, USA) in the dark at room temperature for one hour. The samples were washed three times and exposed to DAPI in the dark at room temperature for 10 minutes. After washing, samples were preserved at 4˚C for confocal microscopy analysis. Images were taken using Leica SP8 confocal system at 10X object (zoom 5).

Confocal microscopy

Images were taken using Leica SP8 confocal system at 10X object (zoom 5) using the LAS X life science microscope software. TIFF files were exported for further analysis. For fluorescence intensity analysis of pCD18 and mAB21, images were converted to binary images in the ImageJ software and intensity was measured using the “Analyze particles” algorithm available in ImageJ.

Dataset analysis using CIBERSORT

Transcriptomic data for breast invasive adenocarcinoma and colorectal adenocarcinoma were obtained from TCGA (Broad GDAC firehose-Broad institute, https://gdac.broadinstitute.org/) and converted to a format compatible with the CIBERSORT software (24). The algorithm was run using a signature gene file (LM22) containing expression data for 22 genes that effectively identify specific immune cell types. Calculated percentages of NK cells computed by this method for tumors and normal tissues were compared using GraphPad Prism.

Immunoprecipitation

NK cells were isolated and activated with IL2 for 96 hours as described above. The cells were collected and washed with ice cold PBS at 4^{o}C (1500 rpm for 10 minutes). A standard immunoprecipitation protocol was followed as described in a previous publication (25). 1 μg of anti-human C3aR (Cat# SC-133172, Santa Cruz Biotechnology) and 1 μg of anti-human CD11a (Cat# 350602, Biolegend) were used in 1 mg of total protein for pulldown. Pulled down eluates were processed for Western blotting as described below.

For mouse NK-cell immunoprecipitation, mouse NK cells were treated with IL2 for 96 hours as described. The activated mouse NK cells were processed as described above. Pulldown assays were performed for C3aR using anti-C3aR ((Cat# SC-133172, Santa Cruz Biotechnology). Polyclonal anti CD11a polyclonal antibody (Cat# BS 20370R, Bioss) and Anti C3aR polyclonal antibody (Cat# BS 2955R, Bioss) were used for immunoblotting.

Immunoblotting

Samples were run in 4–20% Criterion TGX Precast Midi Protein Gel (Bio-Rad Cat# 5671093). Transfer onto a PVDF membrane was performed using Bio-Rad wet transfer with Tris-glycine buffer containing 10% methanol and 0.01% SDS. The membrane was blocked with 5% milk in PBST (0.1% v/v Tween-20) at room temperature for one hour. Primary antibodies were diluted in 5% BSA in PBST and incubation was performed at 4^{o}C overnight. Anti-CD11a (Cat# ab52895, abcam) and polyclonal anti-C3aR (Cat# BS 2955R, Bioss) were used for immunoblotting of human samples. Polyclonal anti-CD11a (Cat# BS 20370R, Bioss) and polyclonal anti-C3aR (Cat# BS 2955R, Bioss) were used for immunoblotting of mouse samples. The membranes were washed with PBST (3X for 10 minutes) and secondary antibody (1:5000 dilution) incubation was performed in 5% milk at room temperature for 1 hour. The membranes were washed and probed with Clarity ECL Western Blotting Substrate (Bio-Rad) or Super Signal West Femto Maximum Sensitivity Substrate (Thermo Scientific) in a ChemiDoc XRS System (Bio-Rad) using Image Lab software (Bio-Rad).

NK-cell cytotoxic assay

50,000 tumor cells (MDA MB-231, HCT116, or CT26) in 100μL were seeded in 96-well plates and cultured for 48 hours. After 48 hours, human or mouse NK cells were added to each well (1:1 ratio of NK and tumor cells; cells were trypsinized from additional wells for cell counting). The mixture was incubated for 4 hours at 37^{o}C in 5% CO_2. The Promega CytoTox 96® Non-Radioactive Cytotoxicity Assay was used according to the provider's procedure (Cat# G1780) The percentage killing was estimated against total lysis.

Statistical analysis

One-way ANOVA was performed if the variable was one independent variable. Two-way ANOVA was performed when there were two nominal predictor variables. The SIDAK model was used to compare set of means, and the TUKEY model was used to compare every mean with every other mean (3 or more sets).

Data availability

The data that support the findings of this study are available within the article and its supplementary data files.

Results

TCGA data show decreased activated NK cell infiltration

Activated NK-cell infiltration into the TME is a marker for better prognosis in a number of solid tumors (9). However, the infiltration of cytotoxic NK cells in solid tumors is generally low. Because previous clinical studies report elevated serum C3a concentration and decreased NK-cell infiltration in invasive breast cancer and colorectal adenocarcinomas, we selected these two tumor types for analysis (26–29). We used CIBERSORT to quantify the differences in mRNAs associated with NK cells as a surrogate means of assessing infiltrating activated NK cells in tumor and normal tissues from TCGA data (24). We first compared NK-cell gene expression changes in 98 normal breast tissues and 250 breast tumor tissues. Activated NK-cell infiltration within total immune cells was 2.7% in normal breast tissues and 0.7% in tumor tissues ($p<0.0001$)(Fig. 1a). We also compared normal colon tissues and colorectal tumor tissues (n=51 each). Activated NK cell infiltration was 0.8% in normal colon tissues and 0.28% in tumor tissues ($p=0.0025$)(Fig. 1b). Although there were differences in the frequency of activated NK cells between normal tissues, activated NK-cell infiltration was significantly decreased in malignant tissues compared to normal tissues. Kaplan Meier survival analysis of TCGA data for invasive breast cancer showed that increased NK-cell infiltration, based on expression of activating NKG2D (*KLRK1*), associated with increased overall survival (Fig. 1c).

Blocking C3aR activity promotes human IL2-activated NK-cell migration

We next investigated C3aR expression on human NK cells. Flow cytometry analysis showed C3aR expression in 75% of total IL2-activated NK cells (Fig. 1d). Building on our analysis of clinical breast and colorectal tumor samples described above, we measured C3a in supernatants from the breast and colorectal tumor cells grown in culture for 48 hours and

found detectable concentrations of C3a in supernatants from MDA-MB-231, MCF7, BT474, and HCT116 cells (Fig. 1e).

To investigate the role of C3aR on NK-cell migration, we performed fibronectin-coated transwell assays and quantified NK-cell migration against conditioned media from tumor cells. The results showed decreased NK-cell migration in presence of conditioned media from MDA-MB-231 and HCT116 cells. Addition of anti-human C3a or blocking of C3aR by SB-290157, a small molecule antagonist of C3aR, resulted in a 3-fold increase of NK-cell migration (Fig. 1f). These results supported a negative role of C3aR on NK-cell migration. We also found that C3a neutralization did not affect NK-cell cytotoxicity against tumor cells (Supplementary Fig. S1a–b).

To further investigate the role of C3aR on NK-cell migration, we performed live cell migration assays in a 2D microfluidic platform. The microfluidic channel was coated with fibronectin and then IL2-activated NK cells were attached (see Methods). These microfluidic-based assays also demonstrated an inhibitory role of C3a on NK-cell migration. Non-polarized NK cells did not migrate in C3a-containing environments (Fig. 2b, 2d, Supplementary Fig. S1c). A control experiment with NK cells exposed to IgG alone showed polarization of NK cells based on pseudopod and uropod formation and increased migration (Fig. 2a, 2c, Supplementary Fig. S1d). The average migration velocity was approximately 3-fold higher in untreated cells compared to C3a-treated cells (Fig. 2e). We also found that NK cells migrated poorly when exposed to supernatants from MDA-MB-231 cells (Fig. 2f, Supplementary Fig. S1e). When a neutralizing antibody against C3a is added to MDA-MB-231 cells, we found significantly increased NK-cell migration and velocity (Fig. 2g-h, Supplementary Fig. S1f). Similar results were obtained for supernatants from HCT116 cells (Fig. 2i-2k, Supplementary Fig. S1g-h).

C3aR inhibition promotes NK cell infiltration into tumors and reduces tumor growth

Because most of the *in vitro* studies were performed in human cells, we needed to first determine if C3aR had similar effects in mouse NK cells. The purity of isolated NK cells from human enriched leukocyte was 95% and 90% from mouse spleen (Supplementary Fig. S2a–b). We confirmed the expression of C3aR on activated NK cells obtained from C57BL/6 mice (Supplementary Fig S2c). The fibronectin-coated transwell assays confirmed the inhibitory role of C3a and C3aR on murine NK-cell migration in the presence of conditioned media from EO771 and MC38 cell lines compared to untreated controls (Supplementary Fig. S2d).

After implanting EO771 tumor cells orthotopically and MC38 tumor cells subcutaneously in C57BL/6 mice and allowing the tumors to reach approximately 100 mm^3 in size (see Methods), we evaluated the role of C3aR on NK-cell exclusion in these tumors by treating with SB-290157 every 12 hours for five days (23). We found significantly decreased tumor growth in SB-290157–treated mice compared to vehicle-- treated mice for both EO771 and MC38 models (Fig. 3a-b, 3e-f). SB-290157–treated animals also exhibited significantly decreased tumor weights compared to vehicle-treated animals (Fig. 3c, 3g). Flow cytometry showed a 2–3–fold increase in NK-cell infiltration in the tumor samples obtained from SB-290157-treated mice (Fig. 3d, 3h, Supplementary Fig. S3). C3aR inhibition showed

no significant difference in T-cell infiltration in E0771 tumors (Supplementary Fig. S4a–b) and increased T-cell infiltration in MC38 tumors (Supplementary Fig. S4c–d), there. Flow cytometry also showed increased infiltration of macrophages with C3aR inhibition in both tumor models (Supplementary Fig. S4e–f). We did not observe weight loss or any abnormalities in the control- or treated-animals. Taken together, these *in vivo* results support a role of C3aR on NK-cell exclusion in the TME. We further investigated the effect of inhibiting C3aR with SB-290157 on NK cell migration using the microfluidic platform. We treated NK cells with or without SB-290157 in the presence of C3a and observed increased velocity in the SB-290157–treated NK cells (Fig. 4a–c).

To investigate the role of NK cells in tumor regression, we performed NK-cell depletion using anti-NK1.1 in the MC38 subcutaneous model (IgG-treated control group included). SB-290157 was administered every 12 hours to the NK1.1- and control-treated groups once the tumors reached approximately 100 mm^3 in size (see Methods). Significantly increased tumor growth in the NK cell–depleted/SB-290157–treated group was seen compared to the SB-290157 alone group, demonstrating the importance of NK-cell infiltration in tumor control (Fig. 4d). SB-290157–treated animals exhibited significantly decreased tumor weights compared to NK cell–depleted/SB-290157–treated animals and vehicle-treated animals (Fig 4e–f). Flow cytometry showed decreased NK-cell infiltration in NK cell–depleted/SB-290157–treated animals compared to IgG/SB-290157–treated group (Fig. 4g, Supplementary Fig. S3). We confirmed the NK-cell depletion in spleens obtained from NK1.1-depleted and control groups (Fig. 4h).

Genetic loss of C3aR facilitates increased infiltration of NK cells into tumors

We also examined the role of C3aR on NK-cell migration using C3aR-KO NK cells. Knockout of C3aR in C3aR-KO animals was confirmed by flow cytometry and PCR (performed PCR as described by the vendor)(Supplementary Fig. S5a–b). In transwell assays, increased migration of wild-type (WT) and C3aR-KO NK cells was observed in the presence of the chemokine CXCL12 (SDF). A 4-fold increase in NK-cell migration from C3aR KO cells was seen compared to WT and controls when C3a was added (Supplementary Fig. S5c). We also found that IL2-activated C3aR-KO NK cells exhibited a 3–4–fold increase in migration compared to WT NK cells in tumor cell conditioned media (Supplementary Fig. S5d). Treatment of WT NK cells with SB-290157 increased NK cell migration and was comparable to that found with C3aR-KO NK cells (Supplementary Fig. S5d). We also examined the role of C3aR in syngeneic JC and CT26 tumor models in BALB/c mice and found that growth of both tumor types was inhibited in C3aR-KO mice compared to WT BALB/c mice (Fig. 5a, 5c). Flow cytometry showed a 2–3-fold increase in NK-cell infiltration in tumors from C3aR-KO mice compared to WT controls (Fig. 5b, 5d, Supplementary Fig. S3). Immune analysis of the tumors also showed no significant difference in the $CD8^+$ T cells and macrophages (Supplementary Fig. S6a, S6c) and an increase in $CD4^+$ T cells in tumors obtained from C3aR-KO animals (Supplementary Fig. S6b). These studies indicate that C3aR mediates inhibition of NK-cell migration and tumor growth in syngeneic mouse models. We also used rabbit polyclonal anti-asialo-GM1 to deplete NK cells and then assessed the effects on tumor regression in C3aR-KO mice. Increased tumor growth in the NK cell–depleted C3aR KO mice was observed compared

to NK cell–infiltrated C3aR-KO tumors (Fig. 5e). Tumor growth in NK cell–depleted BALB/c and NK cell–depleted C3aR-KO mice was similar to saline-treated control BALB/c wild-type mice (Fig. 5e). Flow cytometry of harvested tumors showed elevated NK-cell infiltration only in the saline-treated C3aR-KO mice compared to anti-asialo-GM1–treated and saline-treated groups (Fig. 5f–g). In summary, these results demonstrate a critical role of the C3a/C3aR axis in regulating NK cells and tumor regression.

C3aR activation prevents localization of LFA-1 and alters the LFA-1 conformation

Integrins, specifically LFA-1, plays a critical role in activated NK-cell migration (15,16,21). Using the "STRING" portal, a computational-based method to predict protein-protein interactions (30), we found a strong (90%) interaction between C3aR and the integrin β_2 chain subunit, which typically binds to the integrin α chain subunit CD11a to form LFA-1 (Supplementary Fig. S7a–b). Because LFA-1 is predominantly expressed in cytotoxic NK cells and other β_2 integrins are expressed at reduced levels in NK cells and do not typically participate in NK cell migration, we decided to investigate the role of LFA-1 in cytotoxic NK-cell migration into the TME (18–20). Because β_2 integrin is not exclusively found in LFA-1, we focused on the CD11a subunit, which is specific to LFA-1. We performed reciprocal co-immunoprecipitation (Co-IP) experiments with anti-human C3aR or Co-IP with anti-human CD11a and found that C3aR and LFA-1 co-immunoprecipitated (Fig. 6a).

LFA-1 is activated by outside-in (ligand binding) and inside-out (activation by chemokine receptors and other GPCRs) (31,32) processes. The inside-out activation leads to a high-affinity LFA-1 conformation, exposing epitope 24, in the β_2 subunit, which is otherwise hidden in the inactive (bending) or intermediate active forms (16,33,34), and thus, can be detected with the antibody mAB24 (16). Activation of the β_2 subunit associates with cytoskeletal rearrangement and cell spreading involving α actinin (14,33,35). Inside-out signaling activates the β2 subunit and induces a conformational change in LFA-1, leading to cytoskeletal rearrangement in immune cells (14,33,35–37). The localization of low-affinity LFA-1 at the uropod is critical for efficient immune cell migration, whereas high-affinity LFA-1 inhibits migration (17,38). Immunofluorescence showed that NK cells treated with IgG migrated and had focal localization of LFA-1 in the uropod (Fig. 6b), whereas NK cells exposed to C3a did not migrate and exhibited LFA-1 at the plasma membrane (Fig. 6c). C3a-exposed cells exhibited robust expression of epitope 24, indicating a high-affinity LFA-1 conformation (Fig. 6e, Supplementary Fig S7c) whereas control cells did not demonstrate epitope 24 staining (Fig. 6d). The time to induce a high-affinity LFA-1 conformation varies between attached NK cells and suspended NK cells. Attached NK cells in the microfluidic-based experiments showed a high-affinity conformation immediately after C3a treatment (Fig. 6e). In contrast, suspended NK cells required extended time (3-hour incubation) to demonstrate a high-affinity conformation (Supplementary Fig. S7d). During inside-out signaling, the β2 subunit is activated by phosphorylation at T758 (14,33,35–37). Immunofluorescence showed that T758 was phosphorylated (p-CD18 staining) only in C3a-exposed NK cells, supporting a role for C3a in inside-out signaling through the β2 subunit (Fig 6f–g, Supplementary Fig. S7e). We confirmed the role of C3aR in the high-affinity LFA-1 formation by using SB-290157. Immunofluorescence did not show mAB24 reactivity in the C3a-treated NK cells in the presence of SB-290157 (Supplementary

Fig. S7f). Taken together, these results demonstrate a direct effect of C3a/C3aR on LFA-1 localization in the uropod, β2 integrin phosphorylation, and formation of the LFA-1 high-affinity conformation.

C3a treatment alters LFA-1 conformation in activated NK cells

To investigate the conformational change in LFA-1 in human NK cells, we treated IL2-activated human NK cells to receptor-saturating concentrations of human recombinant C3a. This increased epitope 24 staining, representing activation of domain I in the β2 subunit of LFA-1 and indicating high-affinity LFA-1 conformation (Supplementary Fig. S7d). To confirm the interaction between mouse C3aR and LFA-1, we immunoprecipitated C3aR from lysates of activated NK cells from C57BL/6 mice and probed for CD11a. Results indicated an interaction between C3aR and CD11a (Supplementary Fig. S8a). We also found that C3a increased the high-affinity conformation of LFA-1 in activated NK cells from wild-type mice, whereas C3a incubation did not alter LFA-1 conformation of activated NK cells from C3aR-KO mice, demonstrating a link between C3a/C3aR and the high-affinity formation of LFA-1 (Supplementary Fig. S8b).

Blocking high affinity LFA-1 promotes NK cell migration and infiltration

Previous studies have shown that BIRT 377 acts as an allosteric inhibitor of the high-affinity LFA-1 conformation by blocking domain I in the β2 subunit (38,39). In our microfluidic experiments, inhibition of the high affinity conformation of LFA-1 with BIRT377 significantly increased the migration and velocity of C3a-treated NK cells compared to vehicle-treated cells (Fig. 7a–c, Supplementary Fig. S8c–d). Immunofluorescence also indicated the absence of high-affinity LFA-1 in the BIRT377-treated cells (Fig. 7d). Addition of BIRT377 in MDA-MB-231 supernatants increased the migration and velocity of NK cells exposed to the treated supernatant compared to control supernatant (Supplementary Fig. S8e–i). Taken together, these results revealed the inhibitory role of C3a-induced high-affinity LFA-1 on NK-cell migration. As a follow-up to the *in vitro* studies, we investigated the effect of BIRT377 on NK-cell infiltration and CT26 tumor growth. BIRT377 treatment resulted in significant CT26 tumor regression and increased NK-cell infiltration compared to untreated controls (Fig. 7e–g). Cytotoxicity assays showed that the addition of BIRT377 did not affect the cytotoxicity of activated mouse NK cells (Supplementary Fig. S8j). In summary, these studies demonstrate the requirement for the low-affinity LFA-1 conformation to increase NK-cell infiltration into tumors, which leads to tumor regression.

Discussion

Increased infiltration of cytotoxic NK cells into tumors correlates with a better prognosis and more effective immune response (40,41). In contrast to cytotoxic T cells, NK cells do not require prior priming and have a rapid cytotoxic effect on tumor cells (42). Unfortunately, the majority of solid tumors have low infiltration of NK cells (9). Previous studies have shown that cancer cells can secrete factors that create a suppressive microenvironment for infiltrating NK cells (9).

Only a minority of patients respond positively to immune checkpoint inhibitor therapy because in many cases, tumors lack a sufficient cytotoxic immune population and, therefore, derive little benefit from immune checkpoint inhibitor therapy (43). Hence, it will be important to study the role of checkpoint blockade therapy in modulating NK-cell activity when NK-cell numbers can be therapeutically increased in solid tumors.

Previous studies show increased C3a concentration in various solid tumors and serum samples obtained from human cancer patients (11). Paradoxically, although C3a inhibits NK-cell migration into tumors, C3a is also a chemoattractant for other immune cells (44). IL2 stimulation is sufficient to induce C3aR expression on NK cells. In contrast, cytotoxic T cells require inflammation and type-1 IFNs for C3aR expression (45). Consequently, C3aR expression on other immune cells may vary with the degree of inflammation and local cytokine environment. Therefore, it is critical to study the role of C3aR expression on other immune cells to evaluate this mechanism.

Activated cytotoxic NK cells showed increased LFA-1 expression compared to other β_2 integrins, and this increased expression of both C3aR and LFA-1 inhibited cytotoxic NK-cell infiltration into the TME. Our mouse model experiments demonstrated the importance of the C3aR-LFA-1 axis in the regulation of cytotoxic NK-cell infiltration into TME. LFA-1 expression also varies among immune cells. Unlike $CD56^{dim}$ NK cells, $CD56^{bright}$ NK cells and T cells express decreased LFA-1 (20). Decreased LFA-1 expression may be a reason for the lack of C3a/C3aR-mediated LFA-1 activation in $CD56^{bright}$ NK cells, promoting better $CD56^{bright}$ infiltration into the TME compared to $CD56^{dim}$ cells. The mechanism of LFA-1 activation differs among various immune cells. For example, in T cells, LFA-1 activation requires TCR signaling to induce the inside-out mechanism (19). Unlike NK cells, other immune cells vary in their responses to C3aR stimulation in different tumor models. Therefore, unlike NK cells, where C3aR alone activates LFA-1, other immune cells may require additional signaling to engage C3a/C3aR-mediated LFA-1 activation.

During immune cell migration, LFA-1 translocation to the retracting tail region (uropod) is critical (46). Low-affinity LFA-1 at the uropod promotes decreased adhesion of attached immune cells, facilitating their migration, whereas the high-affinity, active LFA-1 conformation at the uropod promotes adhesion of the uropod, leading to migration arrest (17,47). Our microfluidic-based immunofluorescence experiments demonstrated the inhibitory role of C3a/C3aR in LFA-1 translocation to the uropod. Our results established that C3aR-mediated, inside-out induction of LFA-1 promotes a high-affinity LFA-1 formation. C3aR-KO NK cells had low-affinity LFA-1 formation, resulting in increased NK-cell infiltration into tumors. In T cells, additional signaling through the TCR or chemokine receptors is required to activate LFA-1 for synapse formation. Unlike T cells, NK cells express the intermediate LFA-1 conformation without any external stimuli. The presence of the intermediate LFA-1 conformation in NK cells is sufficient for cytolytic synapse formation through ICAM-1 expressed on target cells (48).

Previous publications have used BIRT377 to promote migration of elongated, non-migrating T cells (46). BIRT337, an allosteric LFA-1 inhibitor, prevents the formation of the high-affinity LFA-1 conformation (39). We confirmed that BIRT377 prevented the formation

of the high-affinity active LFA-1 formation, and found it promoted NK-cell migration and infiltration. BIRT377 treatment, although useful in experimental studies, has some disadvantages, such as decreasing IL2 production, which could preclude it from human use (49). Because high-affinity LFA-1 is indispensable to mediate the synapsis formation between T cells and antigen presenting cells, the use of BIRT377 might result in a T-cell priming defect (50). Due to these limitations and others, it is imperative to develop a tumor-specific approach to target tumor-derived C3a or C3aR on NK cells in order to increase NK-cell infiltration into TME.

In summary, our experimental results define a role of the C3a/C3aR axis in NK-cell exclusion in solid tumors. C3a neutralization or genetic inactivation of C3aR overcomes a seemingly common cytotoxic NK-cell exclusion mechanism, promoting decreased tumor growth. Mechanistically, C3aR interaction with LFA-1 results in a high-affinity LFA-1 conformation, leading to decreased cytotoxic NK-cell infiltration into tumors. Therefore, targeting either the C3a/C3aR axis or inhibiting C3aR interaction with LFA-1 could provide a clinically feasible strategy for NK cell-mediated immunotherapy as a monotherapy or combination with other therapeutic methods.

Supplementary Material

Refer to Web version on PubMed Central for supplementary material.

Acknowledgements

We thank Kaushik Thakkar and Anne Hertz for their support with Western blots and PCR experiments. We thank Kitty Lee and the Stanford Cell Sciences Imaging Facility (CSIF) for their support with confocal microscopy. We thank the Stanford Blood Center for providing human blood samples.

This work was supported by a MRC Grant, and NIH Grants CA-67166, CA-198291 and CA-197713, the Sydney Frank Foundation and the Kimmelman Fund (AG), and NIH Grants CA 67166 and CA197136 (EG). The project described was supported, in part, by Award Number 1S10OD010580–01A1 from the National Center for Research Resources (NCRR). Its contents are solely the responsibility of the authors and do not necessarily represent the official views of the NCRR or the National Institutes of Health.

References

1. Lodoen MB, Lanier LL. Natural killer cells as an initial defense against pathogens. Current Opinion in Immunology 2006;18(4):391–8. [PubMed: 16765573]
2. Larsen SK, Gao Y, Basse PH. NK Cells in the Tumor Microenvironment. Critical reviews in oncogenesis 2014;19(0):91–105. [PubMed: 24941376]
3. Levy EM, Roberti MP, Mordoh J. Natural Killer Cells in Human Cancer: From Biological Functions to Clinical Applications. Journal of Biomedicine and Biotechnology 2011;2011:676198 doi 10.1155/2011/676198. [PubMed: 21541191]
4. Glas R, Franksson L, Une C, Eloranta M-L, Öhlén C, Örn A, et al. Recruitment and Activation of Natural Killer (Nk) Cells in Vivo Determined by the Target Cell Phenotype An Adaptive Component of Nk Cell–Mediated Responses. The Journal of experimental medicine 2000;191(1):129–38. [PubMed: 10620611]
5. Maghazachi A Role of Chemokines in the Biology of Natural Killer Cells. In: Bruserud O, editor. The Chemokine System in Experimental and Clinical Hematology Volume 341, Current Topics in Microbiology and Immunology: Springer Berlin Heidelberg; 2010. p. 37–58.

6. Fogler WE, Volker K, McCormick KL, Watanabe M, Ortaldo JR, Wiltrout RH. NK cell infiltration into lung, liver, and subcutaneous B16 melanoma is mediated by VCAM-1/VLA-4 interaction. The Journal of Immunology 1996;156(12):4707–14. [PubMed: 8648116]
7. Jewett A, Tseng H-C. Tumor induced inactivation of natural killer cell cytotoxic function; implication in growth, expansion and differentiation of cancer stem cells. Journal of Cancer 2011;2:443. [PubMed: 21850212]
8. Albertsson PA, Basse PH, Hokland M, Goldfarb RH, Nagelkerke JF, Nannmark U, et al. NK cells and the tumour microenvironment: implications for NK-cell function and anti-tumour activity. Trends in Immunology 2003;24(11):603–9. [PubMed: 14596885]
9. Lorenzo-Herrero S, López-Soto A, Sordo-Bahamonde C, Gonzalez-Rodriguez AP, Vitale M, Gonzalez S. NK Cell-Based Immunotherapy in Cancer Metastasis. Cancers 2019;11(1):29.
10. Afshar-Kharghan V The role of the complement system in cancer. J Clin Invest 2017;127(3):780–9 doi 10.1172/JCI90962. [PubMed: 28248200]
11. Pio R, Corrales L, Lambris JD. The role of complement in tumor growth. Adv Exp Med Biol 2014;772:229–62 doi 10.1007/978-1-4614-5915-6_11. [PubMed: 24272362]
12. Min X, Liu C, Wei Y, Wang N, Yuan G, Liu D, et al. Expression and regulation of complement receptors by human natural killer cells. Immunobiology 2014;219(9):671–9. [PubMed: 24775270]
13. Shen B, Delaney MK, Du X. Inside-out, outside-in, and inside-outside-in: G protein signaling in integrin-mediated cell adhesion, spreading, and retraction. Curr Opin Cell Biol 2012;24(5):600–6 doi 10.1016/j.ceb.2012.08.011. [PubMed: 22980731]
14. Harjunpää H, Llort Asens M, Guenther C, Fagerholm SC. Cell Adhesion Molecules and Their Roles and Regulation in the Immune and Tumor Microenvironment. Frontiers in Immunology 2019;10(1078) doi 10.3389/fimmu.2019.01078.
15. Dustin ML. Complement Receptors in Myeloid Cell Adhesion and Phagocytosis. Microbiol Spectr 2016;4(6: doi 10.1128/microbiolspec.MCHD-0034-2016.
16. Pouwels J, De Franceschi N, Rantakari P, Auvinen K, Karikoski M, Mattila E, et al. SHARPIN Regulates Uropod Detachment in Migrating Lymphocytes. Cell Rep 2013;5(3):619–28. [PubMed: 24210817]
17. Hind LE, Vincent WJB, Huttenlocher A. Leading from the Back: The Role of the Uropod in Neutrophil Polarization and Migration. Dev Cell 2016;38(2):161–9 doi 10.1016/j.devcel.2016.06.031. [PubMed: 27459068]
18. Bryceson YT, March ME, Ljunggren H-G, Long EO. Activation, coactivation, and costimulation of resting human natural killer cells. Immunological reviews 2006;214:73–91 doi 10.1111/j.1600-065X.2006.00457.x. [PubMed: 17100877]
19. Zhang M, March ME, Lane WS, Long EO. A signaling network stimulated by β2 integrin promotes the polarization of lytic granules in cytotoxic cells. Sci Signal 2014;7(346):ra96-ra doi 10.1126/scisignal.2005629. [PubMed: 25292215]
20. Frey M, Packianathan NB, Fehniger TA, Ross ME, Wang WC, Stewart CC, et al. Differential expression and function of L-selectin on CD56bright and CD56dim natural killer cell subsets. Journal of immunology (Baltimore, Md : 1950) 1998;161(1):400–8.
21. Somersalo K, Tarkkanen J, Patarroyo M, Saksela E. Involvement of beta 2-integrins in the migration of human natural killer cells. The Journal of Immunology 1992;149(2):590–8. [PubMed: 1378070]
22. Rabinowich H, Herberman RB, Whiteside TL. Differential Effects of IL12 and IL2 on Expression and Function of Cellular Adhesion Molecules on Purified Human Natural Killer Cells. Cellular Immunology 1993;152(2):481–98. [PubMed: 7903063]
23. Wang Y, Sun S-N, Liu Q, Yu Y-Y, Guo J, Wang K, et al. Autocrine Complement Inhibits IL10-Dependent T-cell–Mediated Antitumor Immunity to Promote Tumor Progression. Cancer Discov 2016;6(9):1022–35 doi 10.1158/2159-8290.Cd-15-1412. [PubMed: 27297552]
24. Newman AM, Liu CL, Green MR, Gentles AJ, Feng W, Xu Y, et al. Robust enumeration of cell subsets from tissue expression profiles. Nature Methods 2015;12:453 doi 10.1038/nmeth.3337. [PubMed: 25822800]

25. Li CG, Mahon C, Sweeney NM, Verschueren E, Kantamani V, Li D, et al. PPARγ Interaction with UBR5/ATMIN Promotes DNA Repair to Maintain Endothelial Homeostasis. Cell Rep 2019;26(5):1333–43. [PubMed: 30699358]
26. Chung L, Moore K, Phillips L, Boyle FM, Marsh DJ, Baxter RC. Novel serum protein biomarker panel revealed by mass spectrometry and its prognostic value in breast cancer. Breast Cancer Research 2014;16(3):R63 doi 10.1186/bcr3676. [PubMed: 24935269]
27. Mamessier E, Sylvain A, Thibult ML, Houvenaeghel G, Jacquemier J, Castellano R, et al. Human breast cancer cells enhance self tolerance by promoting evasion from NK cell antitumor immunity. J Clin Invest 2011;121(9):3609–22 doi 10.1172/jci45816. [PubMed: 21841316]
28. Halama N, Braun M, Kahlert C, Spille A, Quack C, Rahbari N, et al. Natural Killer Cells are Scarce in Colorectal Carcinoma Tissue Despite High Levels of Chemokines and Cytokines. Clinical Cancer Research 2011;17(4):678–89 doi 10.1158/1078-0432.Ccr-10-2173. [PubMed: 21325295]
29. Habermann JK, Roblick UJ, Luke BT, Prieto DA, Finlay WJJ, Podust VN, et al. Increased serum levels of complement C3a anaphylatoxin indicate the presence of colorectal tumors. Gastroenterology 2006;131(4):1020–284 doi 10.1053/j.gastro.2006.07.011. [PubMed: 17030172]
30. Szklarczyk D, Gable AL, Lyon D, Junge A, Wyder S, Huerta-Cepas J, et al. STRING v11: protein-protein association networks with increased coverage, supporting functional discovery in genome-wide experimental datasets. Nucleic Acids Res 2019;47(D1):D607–D13 doi 10.1093/nar/gky1131. [PubMed: 30476243]
31. Alon R, Dustin ML. Force as a Facilitator of Integrin Conformational Changes during Leukocyte Arrest on Blood Vessels and Antigen-Presenting Cells. Immunity 2007;26(1):17–27. [PubMed: 17241958]
32. Pasvolsky R, Grabovsky V, Giagulli C, Shulman Z, Shamri R, Feigelson SW, et al. RhoA is involved in LFA-1 extension triggered by CXCL12 but not in a novel outside-in LFA-1 activation facilitated by CXCL9. Journal of immunology (Baltimore, Md : 1950) 2008;180(5):2815–23 doi 10.4049/jimmunol.180.5.2815.
33. Fagerholm SC, Hilden TJ, Nurmi SM, Gahmberg CG. Specific integrin α and β chain phosphorylations regulate LFA-1 activation through affinity-dependent and -independent mechanisms. The Journal of Cell Biology 2005;171(4):705–15 doi 10.1083/jcb.200504016. [PubMed: 16301335]
34. Hogg N, Patzak I, Willenbrock F. The insider's guide to leukocyte integrin signalling and function. Nature Reviews Immunology 2011;11(6):416–26.
35. Walling BL, Kim M. LFA-1 in T Cell Migration and Differentiation. Frontiers in immunology 2018;9:952- doi 10.3389/fimmu.2018.00952. [PubMed: 29774029]
36. Abram CL, Lowell CA. The ins and outs of leukocyte integrin signaling. Annu Rev Immunol 2009;27:339–62 doi 10.1146/annurev.immunol.021908.132554. [PubMed: 19302044]
37. Uotila LM, Aatonen M, Gahmberg CG. Integrin CD11c/CD18 α-chain phosphorylation is functionally important. J Biol Chem 2013;288(46):33494–9 doi 10.1074/jbc.C113.497446. [PubMed: 24129562]
38. Morin NA, Oakes PW, Hyun Y-M, Lee D, Chin YE, King MR, et al. Nonmuscle myosin heavy chain IIA mediates integrin LFA-1 de-adhesion during T lymphocyte migration. J Exp Med 2008;205(1):195–205 doi 10.1084/jem.20071543. [PubMed: 18195072]
39. Woska JR Jr., Shih D-t, Taqueti VR, Hogg N, Kelly TA, Kishimoto TK. A small-molecule antagonist of LFA-1 blocks a conformational change important for LFA-1 function. Journal of Leukocyte Biology 2001;70(2):329–34 doi 10.1189/jlb.70.2.329. [PubMed: 11493627]
40. Paul S, Lal G. The Molecular Mechanism of Natural Killer Cells Function and Its Importance in Cancer Immunotherapy. Frontiers in Immunology 2017;8(1124) doi 10.3389/fimmu.2017.01124.
41. Souza-Fonseca-Guimaraes F, Cursons J, Huntington ND. The Emergence of Natural Killer Cells as a Major Target in Cancer Immunotherapy. Trends in Immunology 2019;40(2):142–58. [PubMed: 30639050]
42. Hu W, Wang G, Huang D, Sui M, Xu Y. Cancer Immunotherapy Based on Natural Killer Cells: Current Progress and New Opportunities. Frontiers in Immunology 2019;10(1205) doi 10.3389/fimmu.2019.01205.

43. Darvin P, Toor SM, Sasidharan Nair V, Elkord E. Immune checkpoint inhibitors: recent progress and potential biomarkers. Experimental & Molecular Medicine 2018;50(12):165 doi 10.1038/s12276-018-0191-1.
44. Roumenina LT, Daugan MV, Petitprez F, Sautès-Fridman C, Fridman WH. Context-dependent roles of complement in cancer. Nature Reviews Cancer 2019;19(12):698–715 doi 10.1038/s41568-019-0210-0. [PubMed: 31666715]
45. Werfel T, Kirchhoff K, Wittmann M, Begemann G, Kapp A, Heidenreich F, et al. Activated Human T Lymphocytes Express a Functional C3a Receptor. The Journal of Immunology 2000;165(11):6599–605 doi 10.4049/jimmunol.165.11.6599. [PubMed: 11086104]
46. Capece T, Walling BL, Lim K, Kim K-D, Bae S, Chung H-L, et al. A novel intracellular pool of LFA-1 is critical for asymmetric CD8+ T cell activation and differentiation. The Journal of Cell Biology 2017;216(11):3817–29 doi 10.1083/jcb.201609072. [PubMed: 28954823]
47. Park EJ, Peixoto A, Imai Y, Goodarzi A, Cheng G, Carman CV, et al. Distinct roles for LFA-1 affinity regulation during T-cell adhesion, diapedesis, and interstitial migration in lymph nodes. Blood 2010;115(8):1572–81 doi 10.1182/blood-2009-08-237917. [PubMed: 20023213]
48. Kumar S Natural killer cell cytotoxicity and its regulation by inhibitory receptors. Immunology 2018;154(3):383–93 doi 10.1111/imm.12921. [PubMed: 29512837]
49. Kelly TA, Jeanfavre DD, McNeil DW, Woska JR, Reilly PL, Mainolfi EA, et al. Cutting Edge: A Small Molecule Antagonist of LFA-1-Mediated Cell Adhesion. The Journal of Immunology 1999;163(10):5173–7. [PubMed: 10553036]
50. Wang Y, Li D, Nurieva R, Yang J, Sen M, Carreño R, et al. LFA-1 Affinity Regulation Is Necessary for the Activation and Proliferation of Naive T Cells. Journal of Biological Chemistry 2009;284(19):12645–53 doi 10.1074/jbc.M807207200. [PubMed: 19297325]

Synopsis

Lack of cytotoxic immune cell infiltration into tumors can impact efficacy of therapy. Activation of the C3a receptor is shown to impact cytotoxic NK-cell infiltration into the TME of solid tumors via interactions with the integrin LFA-1.

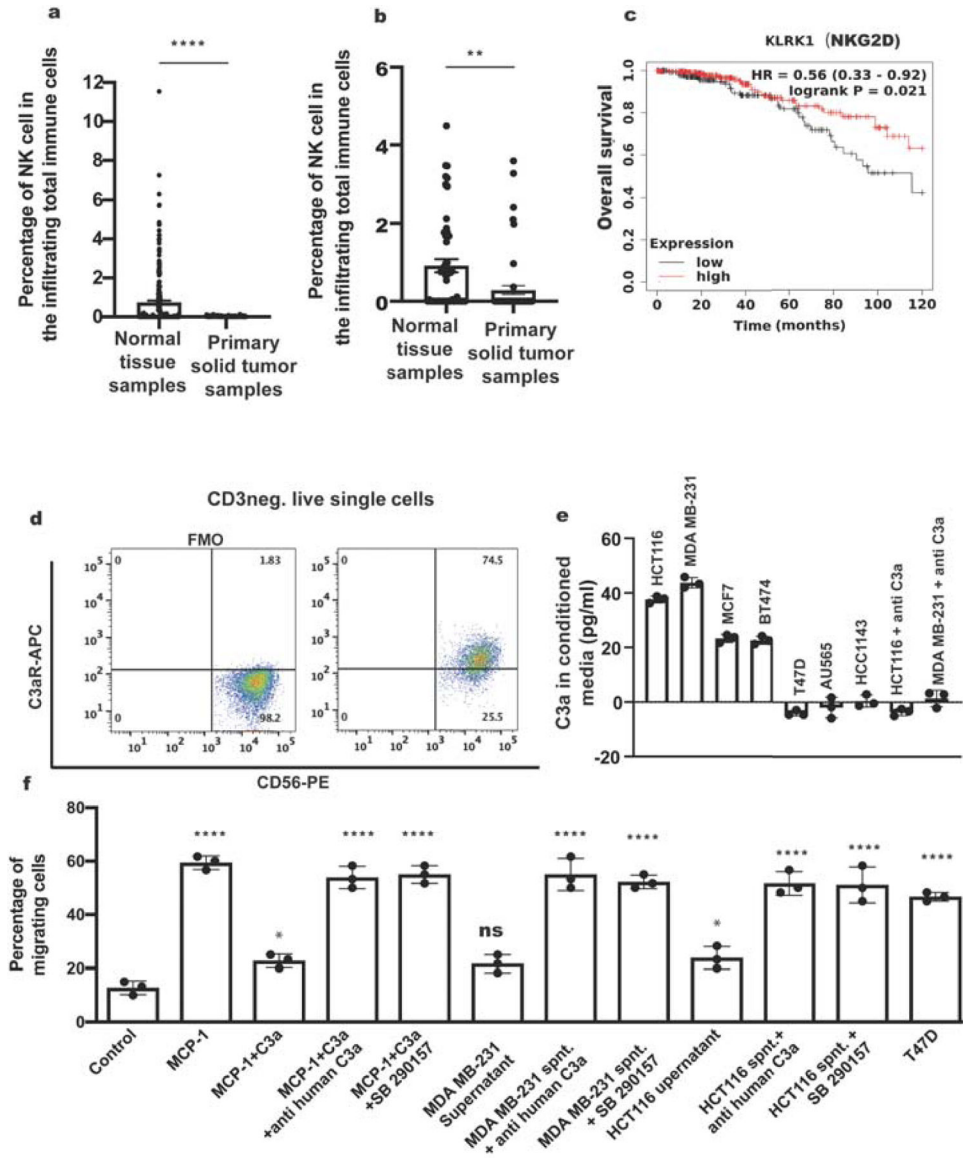

Fig 1. NK cell infiltration in TCGA tissue samples and *in vitro* NK-cell migration.

a-b. CIBERSORT analysis of activated NK cells in TCGA datasets for (a) normal human breast tissue (n=98) compared to invasive breast cancer tissues (n=250) and (b) in human colorectal tissues compared to colorectal adenocarcinomas (n=51 for each tissue). Unpaired two-tailed student t-test. Error bars represent SEM. **c.** Kaplan-Meier curve of overall survival of TCGA breast cancer patients with high and low *KLRK1* mRNA expression. **d.** Scattered plots of C3aR expression in IL2-activated human NK cells. **e.** C3a quantification in conditioned media from the indicated cell lines. **f.** Activated NK-cell migration in fibronectin-coated transwell assays with the indicated treatments compared to controls. (e-f) Test results were compared with control using one-way ANOVA, with Dunnett's multiple comparisons test. *p<0.05, **p<0.01; ***p<0.001; ****p<0.0001, ns: not significant. Error bars represent SD.

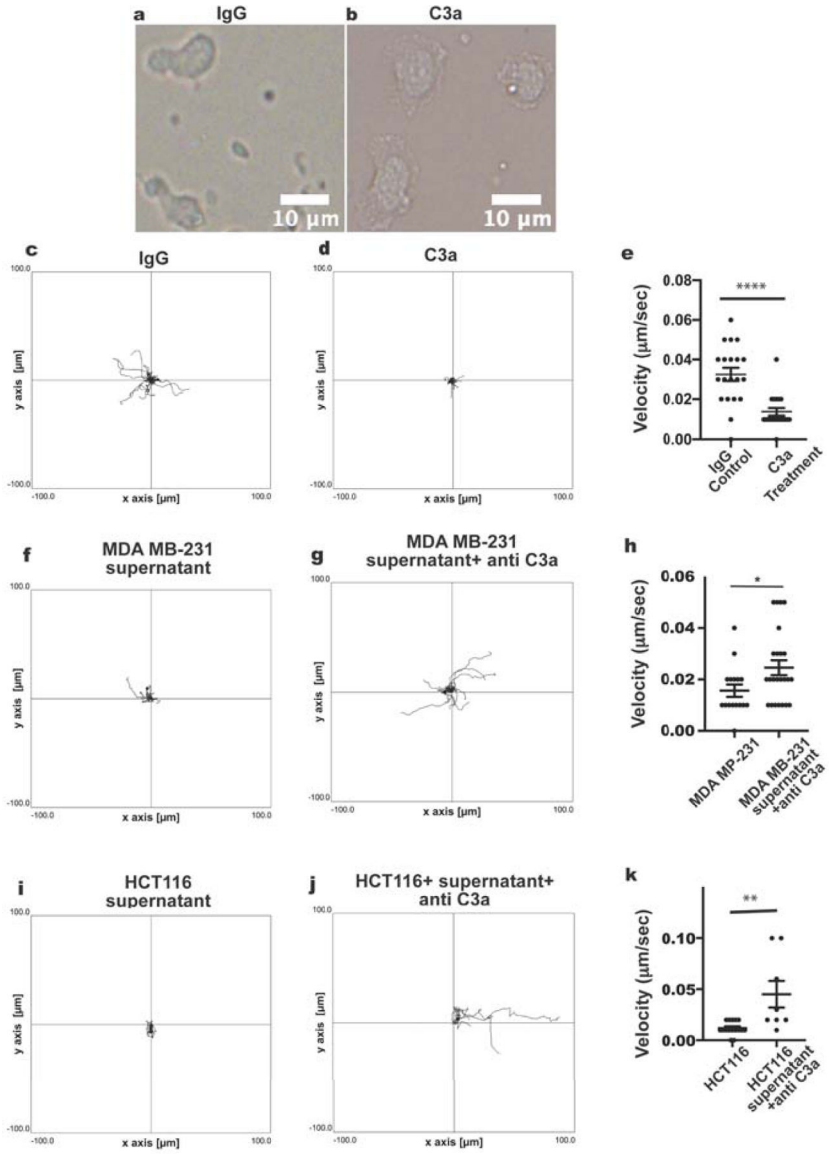

Fig 2. C3a neutralization increases the migration of IL2-activated human peripheral blood NK cells in a 2D microfluidic models.

a-b. Representative images of (a)polarized (pseudopod and uropod), migrating human NK cells and (b) non-polarized (rounded), non-migrating NK cells. Scale bar: 10 µm. **c-e.** NK-cell tracks and velocity in C3a-containing medium and IgG controls. **f-h.** NK-cell tracks and velocity in MDA-MB-231 supernatant with/without C3a neutralization. **i-k.** NK-cell tracks and velocity in HCT116 supernatant with/without C3a neutralization. Velocity comparison was done using an unpaired two-tailed student t-test. Error bars represent SEM. *p<0.05, **p<0.01; ***p<0.001; ****p<0.0001, ns: not significant.

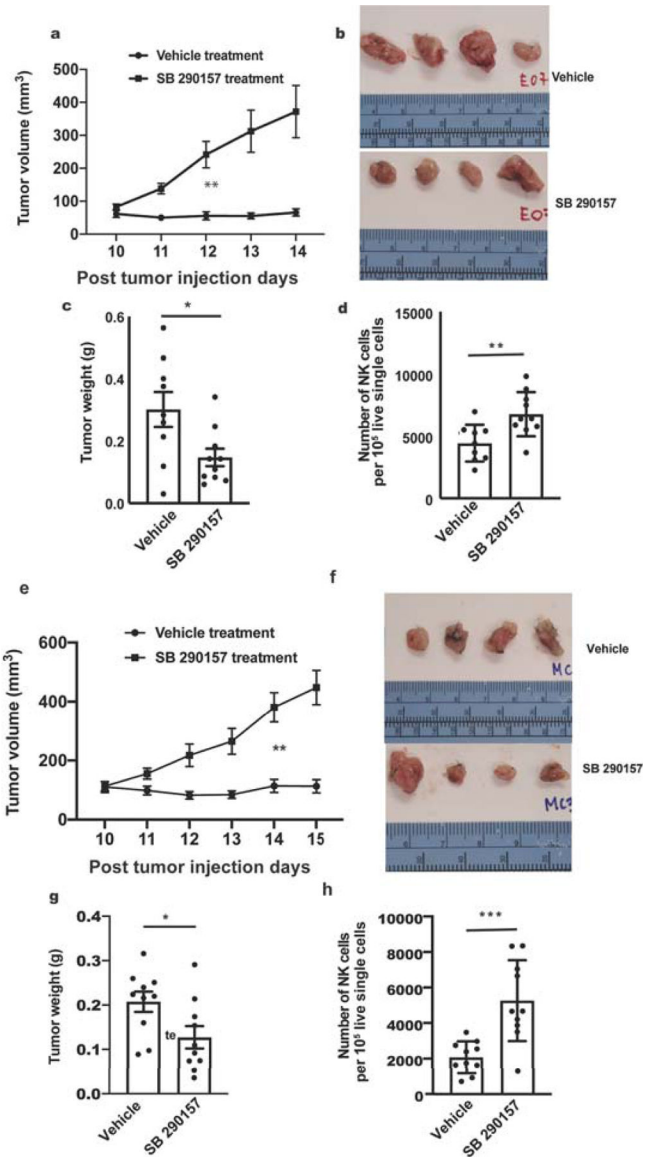

Fig 3. C3aR blocking increased NK-cell infiltration into the EO771 and MC38 TME in C57BL/6 mice.

a, e. EO771 and MC38 tumor growth, respectively, in control and SB-290157-treated mice (n=10/group each). Error bars represent SEM. **b, f.** Representative images of tumor size from control and SB-290157-treated mice. **c, g.** Tumor weight comparison between tumors from control and SB-290157-treated mice. **d, h.** NK-cell infiltration. Comparisons were made using two-way ANOVA employing Sidak's multiple comparisons test for a and e. Comparisons were made using an unpaired two-tailed student t-test for c, d, g, and h. *p<0.05, **p<0.01; ***p<0.001; ****p<0.0001, ns: not significant; error bars represent SEM.

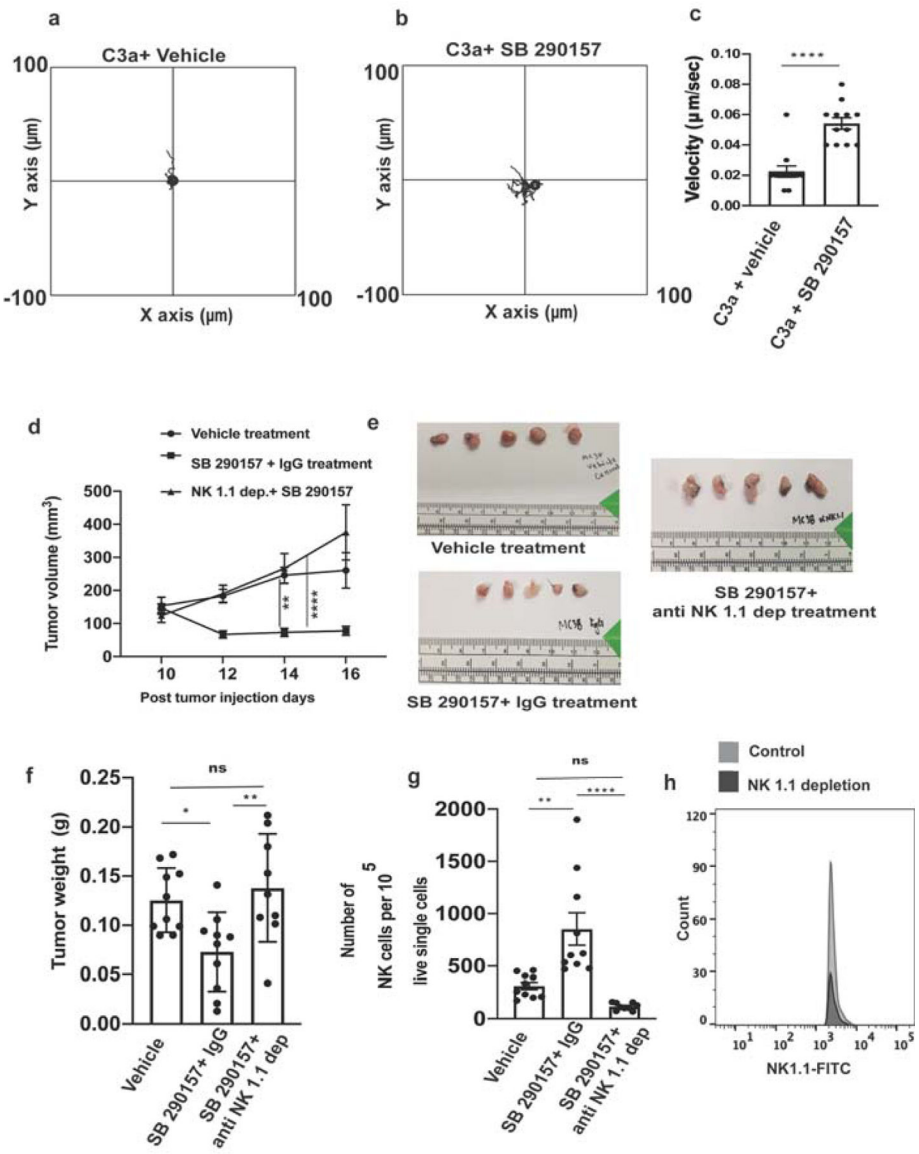

Fig 4. NK-cell depletion increases tumor growth in SB-290157-treated mice.

a-c. NK-cell tracks and velocity in C3a-treated, activated NK cells with or without SB-290157 treatment. **d.** Tumor growth in NK1.1-depleted mice with or without SB-290157 treatment, and saline- and vehicle-treated groups (n=10 in the vehicle control- and SB-290157-treated groups; n=9 in the SB-290157+NK-depleted group). **e.** Representative images of tumor sizes in groups from (d). **f.** Tumor weights among treated groups from (d). **g.** Comparison of NK-cell infiltration in tumors from (d). **h.** Number of splenic NK cells between control and NK1.1-depleted mice from (d). Velocity comparison was done using an unpaired, two-tailed student t-test (error bars represent SD). Tumor growth comparisons were made using two-way ANOVA employing Tukey's multiple comparisons test (error bars represent SEM). *p<0.05, **p<0.01; ***p<0.001; ****p<0.0001, ns: not significant.

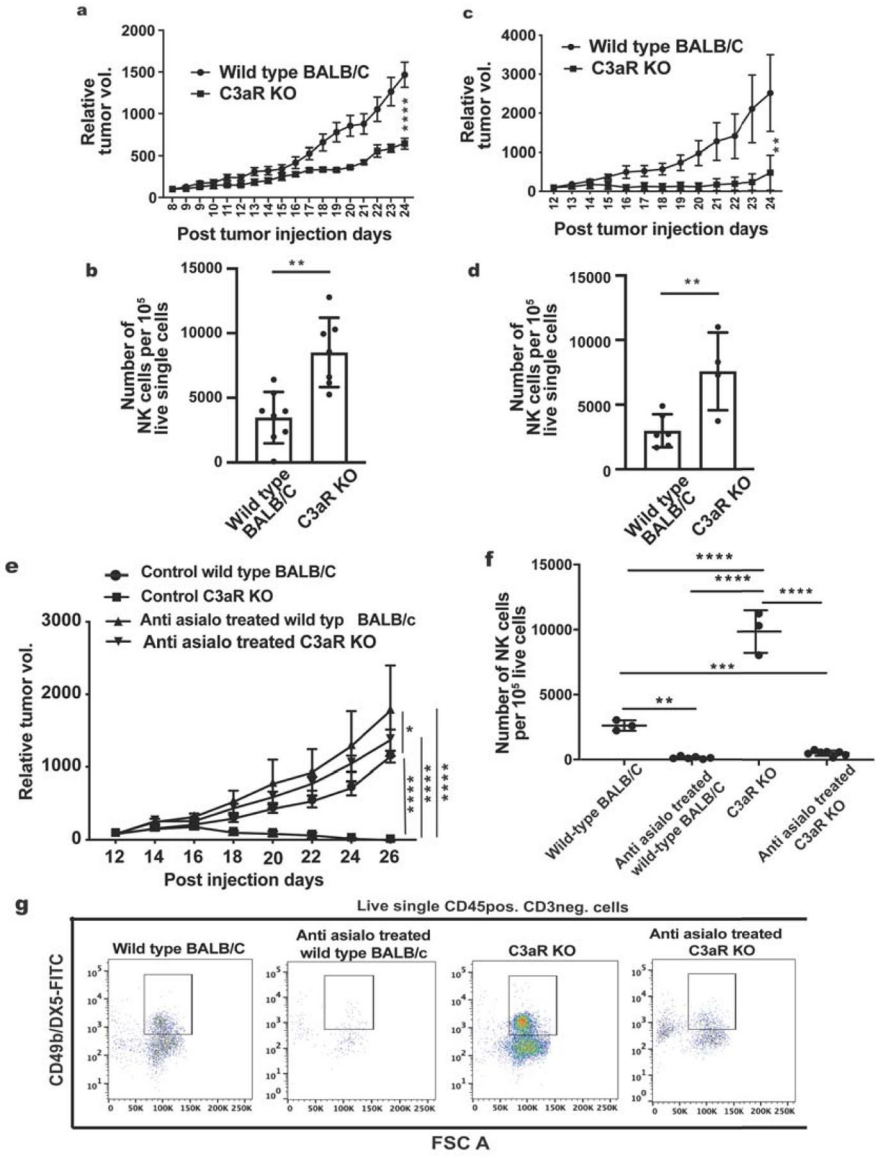

Fig 5: C3aR knockout facilitates increased infiltration of NK cell into syngeneic mouse tumors resulting tumor regression.

a. JC tumor growth in BALB/c wild-type (n=8) and C3aR-KO (n=7) mice. **b.** Quantitation of NK-cell infiltration in (a). **c.** CT26 tumor growth in BALB/c wild-type (n=6) and C3aR-KO (n=5) mice. **d.** Quantification of NK-cell infiltration in (c). The tumor in one antibody-treated animal was too small to isolate for flow cytometry. (a-d) Error bars represent SEM. Comparisons were made using two-way ANOVA employing Sidak's multiple comparisons test for (a, c). Comparisons were made using an unpaired, two-tailed student t-test for (b, d). **e.** CT26 tumor growth in BALB/c wild-type and C3aR-KO mice with and without antibody-mediated depletion of NK cells. (n=7 wild-type, n=8 C3aR-KO; n=7 anti-asialo–treated wild-type, n=8 anti-asialo–treated C3aR-KO). Tumors in 5 C3aR-KO animals were too small to isolate for flow cytometry. Error bars represent SEM. Comparisons were made using two-way ANOVA employing Tukey's multiple comparisons test. **f.** Quantification of NK-cell infiltration in (e). Comparisons were made using an unpaired, two-tailed student

t-test. **g.** NK-cell infiltration in CT26 tumors in BALB/c wild-type and C3aR-KO mice with and without antibody-mediated depletion of NK cells from (e). Error bars represent SEM. *p<0.05, **p<0.01; ***p<0.001; ****p<0.0001, ns: not significant.

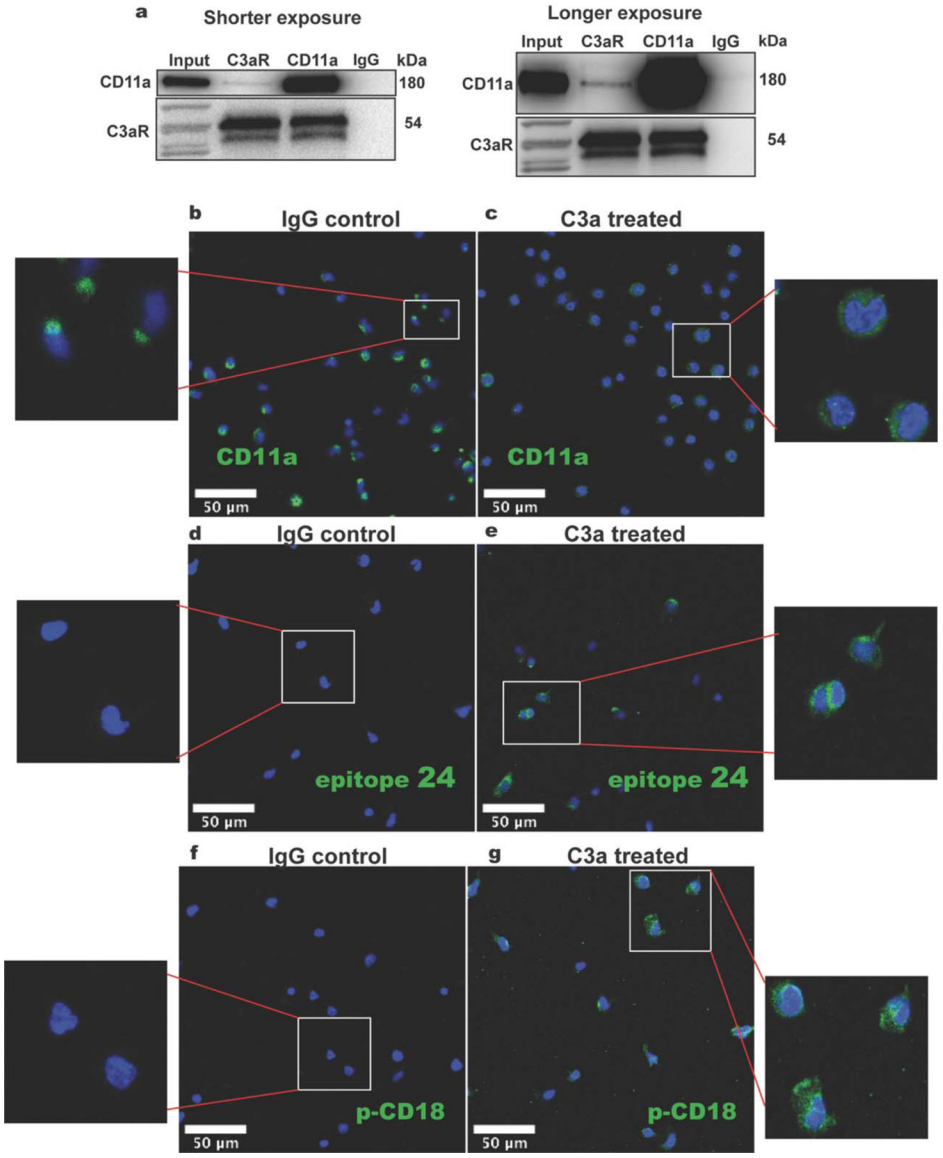

Fig 6. Interactions between stimulated C3aR and LFA-1 facilitate formation of the high-affinity LFA-1 conformation.

a. Immunoprecipitation to assess interaction between C3aR and CD11a (αL subunit that is specific to LFA-1)(n=2). **b, c.** Representative CD11a staining in activated human NK cells with or without C3a stimulation (n=3). **d, e.** Representative LFA-1 epitope 24 staining in activated human NK cells with or without C3a stimulation (n=3). **f, g.** Phospo-CD18 (T758) staining with or without C3a stimulation (n=3). Scale bar: 50 μm. Boxed areas indicate area shown in zoomed images.

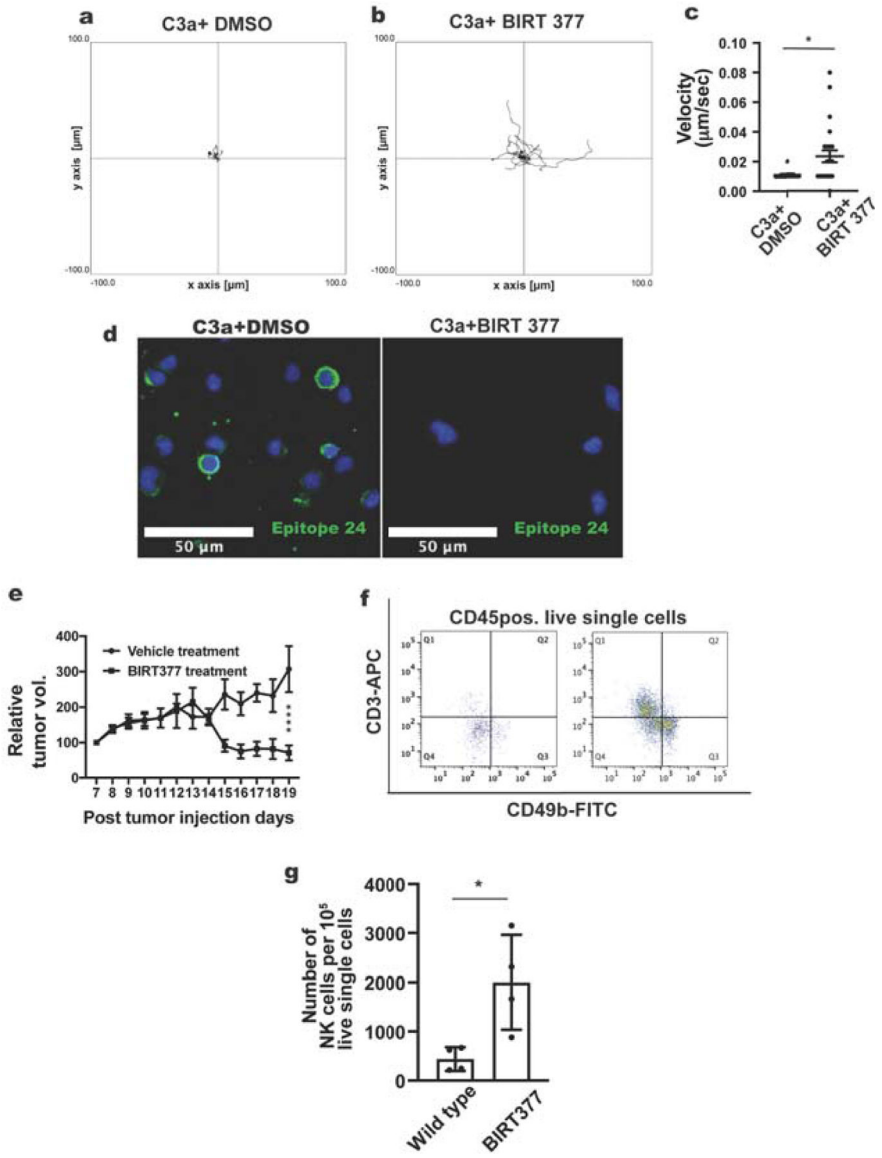

Fig 7. The effect of low-affinity LFA-1 on NK-cell infiltration into the TME in a syngeneic mouse tumor model. C3aR KO facilitates increased cytotoxic NK-cell infiltration into the TME.

a, b. NK-cell tracks from C3a+DMSO control and C3a+BIRT377 experiments. **c.** Velocity between C3a+DMSO control and C3a+BIRT377 experiments. Velocity comparison was done using an unpaired, two-tailed student t-test. **d.** mAB24 staining in C3a+DMSO control and C3a+BIRT377-treated NK cells. **e.** CT26 tumor growth in vehicle-treated and BIRT377-treated wild-type BALB/c mice (n=4/group). Error bars represent SEM. Comparisons were made using two-way ANOVA employing Sidak's multiple comparisons test. **f.** NK-cell infiltration in CT26 tumors in vehicle-treated and BIRT377-treated wild-type BALB/c mice from (e). **g.** Quantification of NK-cell infiltration in (e). Comparisons were made using an unpaired, two-tailed student t-test. *p<0.05, **p<0.01; ***p<0.001; ****p<0.0001, ns: not significant.